Check for updates

The electronic, magnetic, and optical properties of double perovskite La$_2$BB′O$_6$ (B = Cr, V and B′ = Co, Ni and Sc)

Suneela Arif ![ID] * and Yasir Ali ![ID]

2D La$_2$BB′O$_6$ (B = Cr, V and B′ = Co, Ni and Sc) double perovskites are considered promising potential materials for electronic, magnetic, and optoelectronic applications. Herein, we thoroughly investigated the ground state electronic, magnetic, and optical properties of half-metallic ferromagnetic (HM-FM) La$_2$BB′O$_6$ (B = Cr, V and B′ = Co, Ni and Sc) double perovskites using the full-potential linearized augmented plane wave (FP-LAPW) method within the generalized gradient (GGA) and (GGA (+U)) approximations based on density functional theory (DFT). Full structural optimization was carried out by using the FP-LAPW method. The electronic band structure (BS) and the total density of states (DOS) calculations confirm that all these double perovskite compounds are half-metallic (HM). The total spin magnetic moments calculated confirm the half metallic and ferromagnetic nature of the materials. Optical properties were determined for their potential use in opto-electronic devices. Based on our results, we concluded that La$_2$CrCoO$_6$, La$_2$CrNiO$_6$, La$_2$ScNiO$_6$, La$_2$VNiO$_6$ and La$_2$VScO$_6$ compounds are half metal ferromagnetic and have potential applications as ferromagnetic insulators in spintronic, magnetic and optoelectronic devices.

1. Introduction

Perovskites are extensively studied oxides, and exhibit potential applications as insulators/dielectrics in superconductors and a range of materials from diamagnetic to colossal magneto-resistive (CMR).[1–3] BaTiO$_3$ and PbZrO$_3$ are well-known perovskites used in the piezoelectric, dielectric, optoelectronic and microelectronic industries.[4–6] Among the different classes of perovskites are ordered double perovskites (ODP), general formula, A$_2$B′B″O$_6$, where "A" is a rare-earth or alkaline-earth element, while B′ and B″ are different transition-metal ions. These have attracted attention due to their ability to accommodate an extensive range of rare earth elements at the A-site, significantly modifying the bond length and bond angle of the octahedra, and two different types, sizes and valence states of cations at the B′ and B″-sites, offering the opportunity to manipulate, tune and tailor their physical properties according to industrial and technological needs.[7,8] ODP usually exhibit half-metallic (HM),[9,10] ferrimagnetic (FiM),[11,12] ferromagnetic (FM),[13,14] antiferromagnetic (AF),[15,16] half-metallic ferromagnetic (HM-FM),[17,18] half-metallic ferrimagnetic (HM-FiM),[17,19] nonmagnetic (NM),[18,20] ferroelectric (FE),[12,21] and semiconducting (SC)[12,18,21] responses near room temperature. Half-metallic materials have well-defined band gaps in one spin state and metallic bands in the other spin channel.[21] Thus, HM

materials have quantization of magnetic moment, zero spin susceptibility and 100% spin polarization at the Fermi level.[21–23] HM materials have potential application in data storage memory and magnetic recording due to their single spin charge carriers.[24,25] J. B. Philipp *et al.*[26] reported the structural, transport and optical properties and doping effects in half-metallic double perovskites (HM-DP) A$_2$CrWO$_6$ with A = Sr, Ba and Ca. The saturation magnetization and the influence of steric effects on the Curie temperature, T_C, were determined by changing the alkaline earth ion on the A site and a maximum Curie temperature (T_C = 458° K) was reported for Sr$_2$CrWO$_6$, which has an almost undistorted perovskite structure and a tolerance factor $T_f \approx 1$. The researchers showed that the structural changes in Ba$_2$CrWO$_6$ and Ca$_2$CrWO$_6$ result in a reduction of the Curie temperature, suggesting that, in general for double perovskites, an optimal T_C can be achieved only for $T_f \approx 1$. Furthermore, they found that both the Curie temperature and saturation magnetization M_S reduce due to electron doping in Sr$_2$CrWO$_6$ by partial substitution of Sr^{2+} by La^{2+}. Room temperature colossal magneto resistance and high temperature T_C transition for Sr$_2$FeMoO$_6$ systems confirm half-metallic (HM) behavior. Half-metallic ferromagnetic (HM-FM) nature is observed for La$_2$CrCoO$_6$ (LCCO),[27] La$_2$CrNiO$_6$ (LCNO),[28] La$_2$ScNiO$_6$ (LSNO),[27] La$_2$VNiO$_6$ (LVNO)[27] and La$_2$VScO$_6$ (LVSO)[27] compounds, validating their potential suitability for spintronic applications such as in magnetic sensors, magneto resistive random-access memory (MRRAM) and solid fuel cells. A half-metallic antiferromagnetic (HM-AFM) response is observed in LaAVRuO$_6$ (A =

Department of Physics and Astronomy, Hazara University, Garden Campus (Main Campus), Mansehra, Pakistan. E-mail: suneela@hu.edu.pk; Tel: +92 310-050-7841

Ca, Sr, and Ba) systems using the local spin-density approximation (LSDA).[29] Chen et al.[30] reported that La_2VMnO_6 has half-metallic antiferromagnetic (HM-AFM) and ferromagnetic (HM-FM) phases and the antiferromagnetic phase is more stable by 0.1 eV per cell than the ferromagnetic phase. The magneto resistance (MR) in ordered and disordered double perovskite oxide Sr_2FeMoO_6 was investigated by D. D. Sarma et al.[31] They concluded that the ordered sample exhibits a sharp low-field response, followed by moderate changes at higher fields, and the disordered sample was characterized in the absence of a low-field response, confirming that the low-field response depends critically on the half-metallic ferromagnetism, while the high-field response depends on the overall magnetic nature of the sample, still in the absence of the half-metallic state. Although double perovskites are widely studied materials due to their potential applications, no detailed theoretical and experimental studies are available for La based $La_2BB'O_6$ (B = Cr, V and B' = Co, Ni and Sc) double perovskite compounds. Herein, we conclusively theoretically predict the structural, electronic, magnetic and optoelectronic properties of $La_2BB'O_6$ (B = Cr, V and B' = Co, Ni and Sc) double perovskites using first principle generalized gradient GGA[32–34] and GGA (+U)[35,36] approximation calculations, considering the ferromagnetic state in the tetragonal structure (14/mmm, No. 139). Since $La_2BB'O_6$ (B = Cr, V and B' = Co, Ni and Sc) double perovskites are strongly electron correlated systems requiring enhanced description, GGA calculations were corrected by using a strong-correlation correction GGA (+U). We revealed that the electronic magnetic and optoelectronic properties of these materials support their potential use in capacitors, photocells, data storage devices and automobile license plates.

2. Method of calculation

We performed structural, electronic, magnetic and optical property calculations for $La_2BB'O_6$ (B = Cr, V and B' = Co, Ni and Sc) double perovskite compounds using GGA[32–34] and GGA (+U)[35,36] (hybrid term) techniques within the framework of density functional theory (DFT).[37,38] Full structural optimization was carried out by using the full-potential linearized augmented plane wave (FP-LAPW) method[39,40] as implemented in WIEN2K software[41] (updated UNIX versions of the original Wien2K code are called Wien93, Wien95 and Wien97). The WIEN2K software was used to calculate the lattice parameter, band structure, charge density and exchange-correlation potential (V_{Exc}). The charge density and potential were extended in terms of spherical harmonics inside the muffin-tin spheres in terms of the augmented plane wave (APW)[32–36] outside the muffin-tin spheres. In WIEN2K, the basis set APW+ local is used inside the atomic sphere for chemically important orbitals, while FP-LAPW is used for others, therefore it is based on the combination of both techniques.[39–41] The strong electron correlation systems, such as transition metal oxides, were described by the on-site electron correlation correction GGA (+U) method.[35,36] The main control of the convergence in co-relation with the basis size is by means of the parameter, RK_{max}, the product of the largest plane wave vector (K_{max}), the smallest radius of the

sphere (R) and the cutoff value of the angular momentum (L_{max}). In our calculations, for excellence convergence of the charge, a plane wave cut-off value of $R_{MT}K_{max} = 6$ is used in the interstitial region, up to 120 K-point numbers were used for the Brillouin zone for the 14/mmm structures and $L_{max} = 6$ was used for the charge density and potential.

3. Results and discussion

3.1. Electronic band structures and density of states

The band structure (BS) and density of states (DOS) give information about the electronic properties[27,28,36] of the materials, and were investigated using GGA and GGA (+U) for the $La_2BB'O_6$ (B = Cr, V and B' = Co, Ni and Sc) double perovskite systems, as illustrated in Fig. 1 and 2. We observed that the band structures are crowded in both the valence and conduction band. GGA calculations for the La_2CrCoO_6, La_2CrNiO_6, La_2ScNiO_6, La_2VNiO_6 and La_2VScO_6 systems (Fig. 1(a–j) and Table 1) reveal overlapped valence and conduction bands around the Fermi level in spin-up states with a metallic response, whereas in the spin-down channel there was no overlapping around the Fermi level and energy gaps of 0.94 eV, 1.14 eV, 1.63 eV, 1.22 eV and 3.53 eV were exhibited, confirming a non-metallic semi-conducting response, validating half-metallic (HM) behavior in good agreement with previously reported work.[37–39]

Fig. 2(a–j) represent the GGA (+U) calculations for the La_2CrCoO_6, La_2CrNiO_6, La_2ScNiO_6, La_2VNiO_6 and La_2VScO_6 compounds, showing that in the spin-down channel the energy gaps for these compounds were 1.66 eV, 1.21 eV, 3.85 eV, 2.00 eV and 3.56 eV, respectively. However, overlapped valence and conduction bands are observed in the spin-up channel, confirming the metallic response. Both the values of the band gap calculated via GGA and GGA (+U) calculations listed in Table 1 and represented in Fig. 1 and 2 indicate that La_2CrCoO_6, La_2CrNiO_6, La_2ScNiO_6, La_2VNiO_6 and La_2VScO_6 are direct bandgap materials since the maxima of the valence bands and minima of the conduction bands lie at the sigma (Γ) symmetry points.

The band structure calculated by GGA and GGA (+U) shows that the width of the band gaps increases by a specific amount of energy (0.5 eV). The band gap or energy gap (E_g) calculated for La_2VScO_6 is the maximum and equal to 3.537 eV and 3.566 eV whereas La_2CrCoO_6 has the minimum bandgap of 0.945 eV (according GGA), and the La_2CrNiO_6 system has the minimum band gap of 1.211 eV (according to GGA (+U)). The calculated band gaps in terms of electron volts (eV) using GGA and GGA (+U) calculations are illustrated in Table 1 and are in good agreement with other previously reported theoretical work.

The behaviors of the band structures and electronic distributions (states) of the La_2CrNiO_6, La_2ScNiO_6, La_2VNiO_6 and La_2VScO_6 compounds were calculated by total DOS (TDOS) using the GGA and GGA (+U) schemes as shown in Fig. 3 and 4(a–e). The TDOS calculations reveal that in all the compounds a maximum contribution above the Fermi level (E_F), arises due to Tot-La in the spin-up as well as spin-down states. The valence and conduction bands overlapping in the spin-up channel validates the metallic behavior, whereas there is a clear gap between the valence and conduction bands for the spin-down
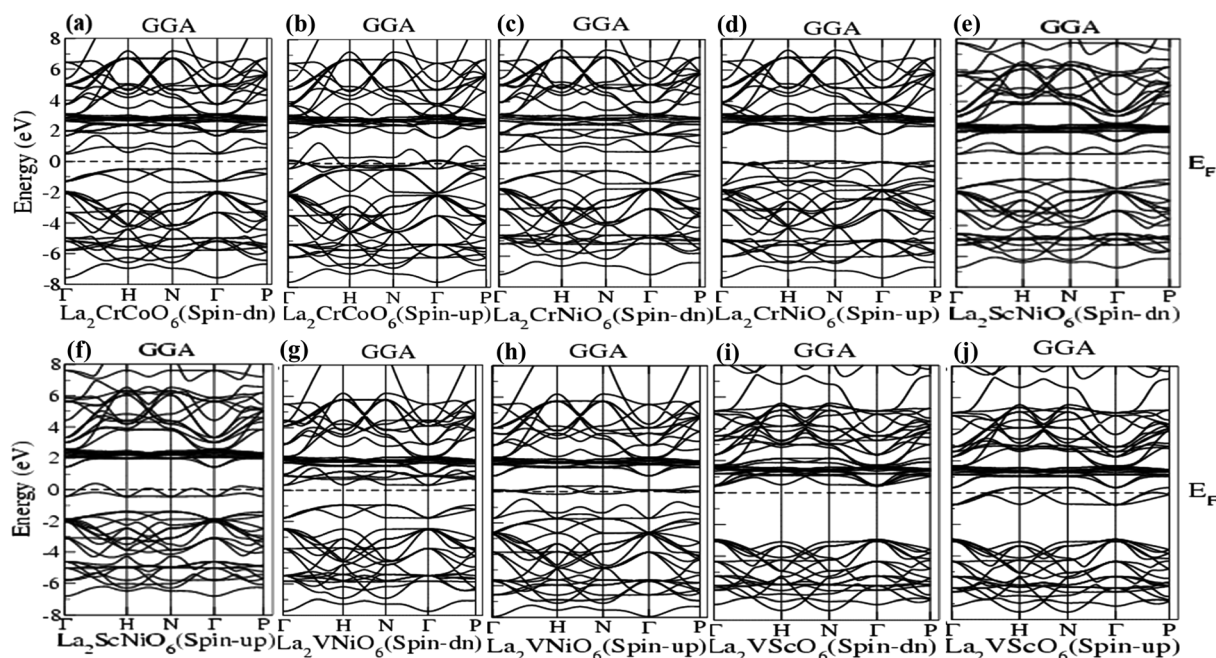
Fig. 1 (a–j) Band structures of La$_2$CrCoO$_6$ (LCCO), La$_2$CrNiO$_6$ (LCNO), La$_2$ScNiO$_6$ (LSNO), La$_2$VNiO$_6$ (LVNO) and La$_2$VScO$_6$ (LVSO) using the GGA scheme.

channel displaying semiconducting behavior, hence confirming that all these compounds are half-metallic. The main reasons for the half metallicity are p–d hybridization and double exchange. The stronger p–d hybridization in these compounds leads to the p-state being pushed above the Fermi level (E_F) in the spin-up channel, while the band extends in the spin-down

channel with E_F exhibiting the double exchange effect, referred to as half-metallicity. In the case of La$_2$CrNiO$_6$ (Fig. 3(b) and 4(b)) in both the spin-up and spin-down channels above the Fermi level, La-f has the maximum contribution, whereas below the Fermi level there is a small contribution from Cr-d and Ni-d to the total density of states (TDOS) and the peak value of the
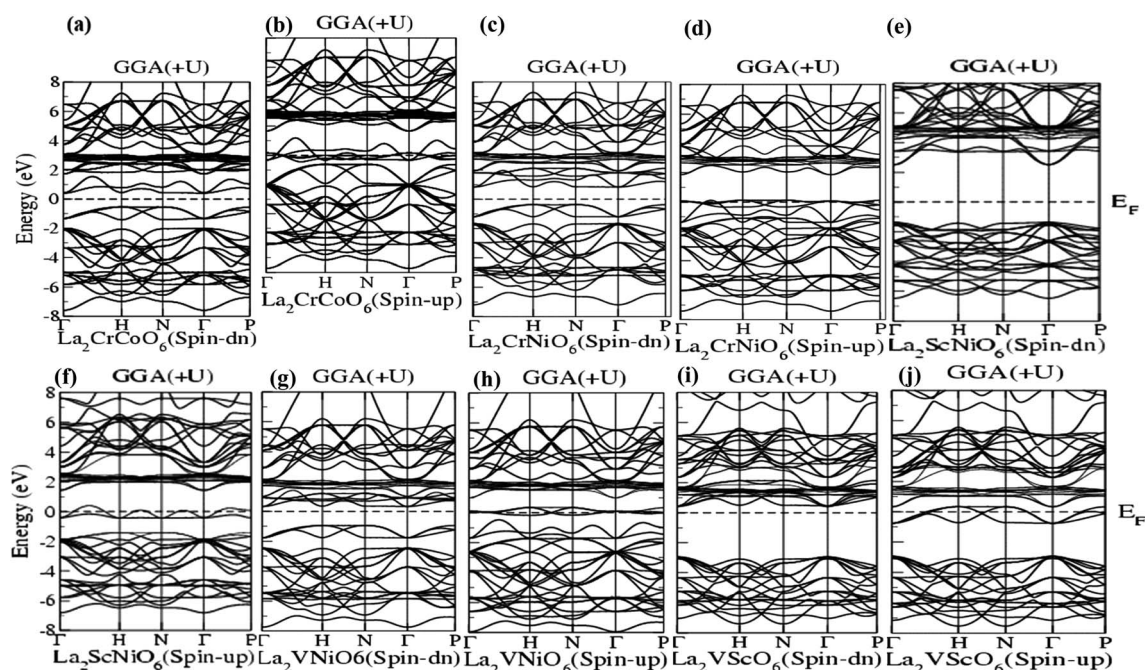

Fig. 2 (a–j) Band structure of La$_2$CrCoO$_6$ (LCCO), La$_2$CrNiO$_6$ (LCNO), La$_2$ScNiO$_6$ (LSNO), La$_2$VNiO$_6$ (LVNO) and La$_2$VScO$_6$ (LVSO) using the GGA (+U) scheme.

Table 1 Spin-up and spin-down state values of the bandgap of La$_2$CrCoO$_6$ (LCCO), La$_2$CrNiO$_6$ (LCNO), La$_2$ScNiO$_6$ (LSNO), La$_2$VNiO$_6$ (LVNO) and La$_2$VScO$_6$ (LVSO) compounds calculated *via* GGA and GGA (+U)

Serial no.	Compound	Spin	Present work E_g (eV)		Other theoretical work E_g (eV)	
			GGA	GGA (+U)	GGA	GGA (+U)
1	La$_2$CrCoO$_6$	Spin-up	Metallic	Metallic	Metallic	Metallic
		Spin-down	0.945296	1.667336	0.94 (ref. 28)	0.762 (ref. 27)
2	La$_2$CrNiO$_6$	Spin-up	Metallic	Metallic	Metallic	Metallic
		Spin-down	1.149897	1.211155	1.14 (ref. 28)	1.007 (ref. 27)
3	La$_2$ScNiO$_6$	Spin-up	Metallic	Metallic	Metallic	Metallic
		Spin-down	1.632651	3.855420	1.63 (ref. 28)	1.497 (ref. 27)
4	La$_2$VNiO$_6$	Spin-up	Metallic	Metallic	Metallic	Metallic
		Spin-down	1.225672	2.00800	1.22 (ref. 28)	1.116 (ref. 27)
5	La$_2$VScO$_6$	Spin-up	Metallic	Metallic	Metallic	Metallic
		Spin-down	3.537194	3.566456	3.53 (ref. 28)	3.238 (ref. 27)

TDOS in the conduction band is nearly 48 (states per eV) at 3 eV. Similarly, we observed that in the case of the La$_2$ScNiO$_6$, La$_2$-VNiO$_6$ and La$_2$VScO$_6$ compounds (Fig. 3(c–e) and 4(c–e)) there is a small contribution of Ni-d to the total density of states (TDOS) below the Fermi level (E_F), while above the Fermi level there is a maximum contribution of La-f to the (TDOS). Furthermore, there is a negligible contribution of O-p to the total density of states (TDOS) below the Fermi level and a small contribution of Sc-d and V-d in the conduction bands, for both the spin-up and spin-down channels.

The DOS is nearly the same for both the GGA and GGA (+U) calculations and the maximum value of the density of states above the Fermi level is at approximately 1.25 eV.
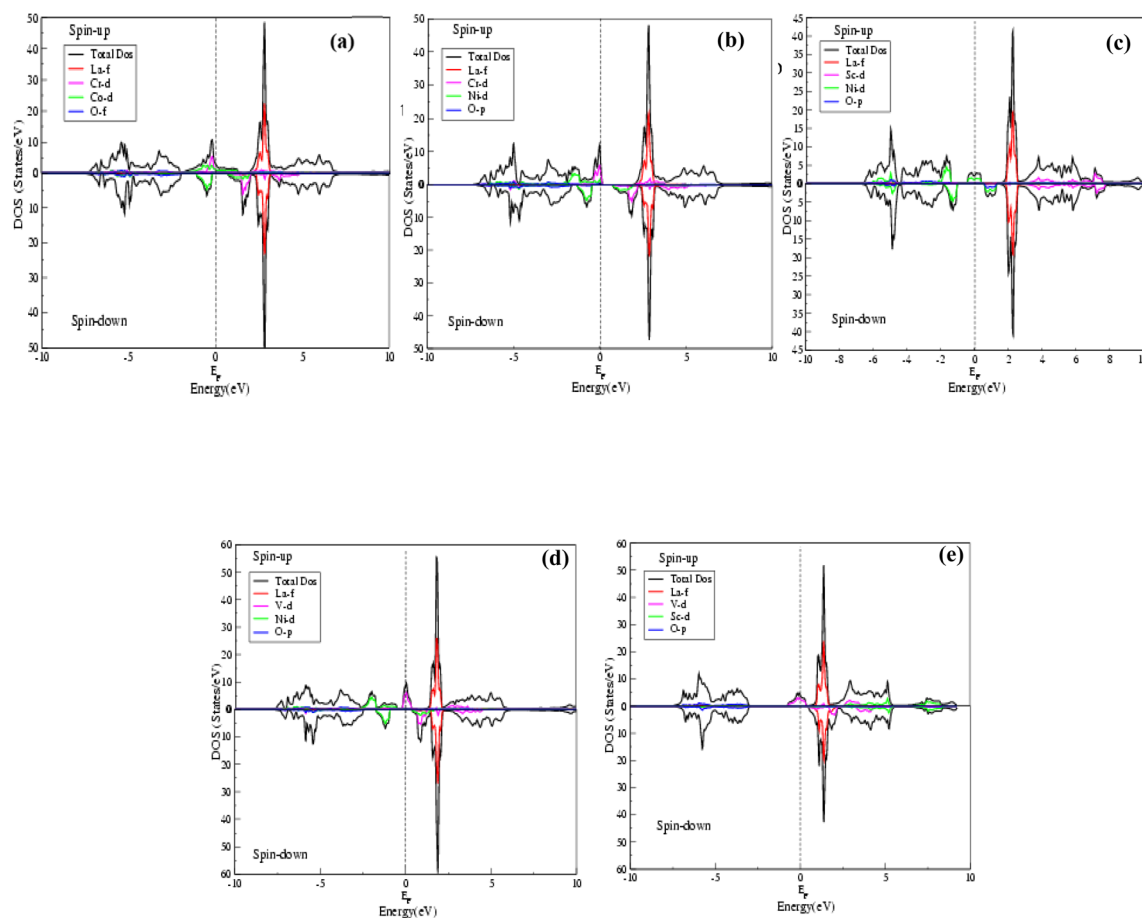
Fig. 3 (a–e) Total density of states (TDOS) of La$_2$CrCoO$_6$ (LCCO), La$_2$CrNiO$_6$ (LCNO), La$_2$ScNiO$_6$ (LSNO), La$_2$VNiO$_6$ (LVNO) and La$_2$VScO$_6$ (LVSO) compounds calculated by the GGA scheme.
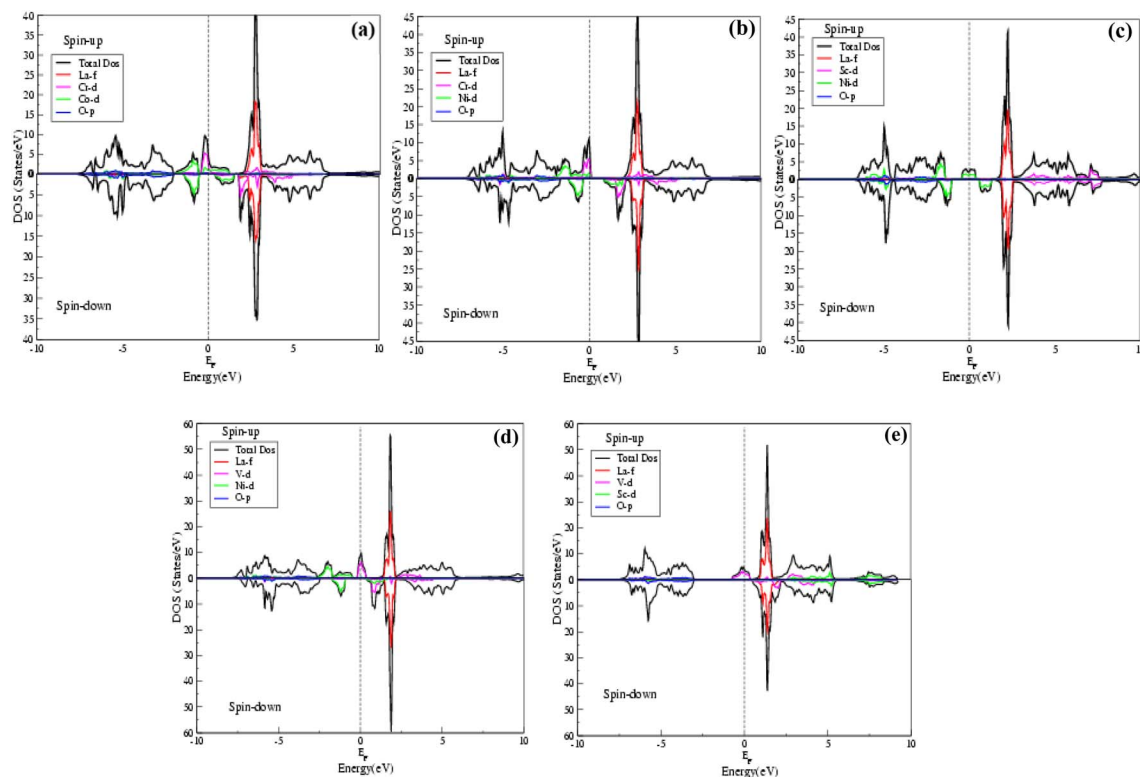
Fig. 4 Total density of states (TDOS) of La_2CrCoO_6 (LCCO), La_2CrNiO_6 (LCNO), La_2ScNiO_6 (LSNO), La_2VNiO_6 (LVNO) and La_2VScO_6 (LVSO) compounds calculated by the GGA (+U) scheme.

3.2. Magnetic properties

The magnetic behaviors of the La_2VNiO_6, La_2VScO_6, La_2ScNiO_6, La_2CrNiO_6 and La_2CrCoO_6 double perovskite compounds were calculated by spin polarized GGA and GGA (+U) approximations by calculating the interstitial region (m^{Intst}), individual atom ($m^{S1, S2, S3, S4}$) and total cell (m^{Cell}) magnetic moments. The detailed values of the magnetic moments calculated are listed in Tables 2 and 3. In the generalized gradient approximation calculation, spinel compound transition metal d-state electrons with oxides are not strongly correlated, which keeps them near the Fermi level (E_F). Therefore, for the transition metal d-state electrons we used GGA (+U) calculations with the U parameter changing from 1.5 eV to 3.0 eV. Choosing an appropriate value of U (ranging from 1.5 eV to 3.0 eV), splits the band structure of these compounds but the total magnetic moments remain the same and the energy gaps increase from 1.2 eV, 3.5 eV, 1.6 eV, 1.1 eV and 0.9 eV to 2.0 eV, 3.6 eV, 3.3 eV, 2.9 eV and 1.6 eV in

spin-down channels. The detailed values of the magnetic moments calculated *via* the GGA and GGA (+U) approximations of all these compounds are illustrated in Tables 2 and 3, and confirm the half-metallic ferromagnetism.

The transition metals Cr, Co, Ni, Sc, and V have the maximum contribution to the total spin magnetic moments, whereas La has the minimum contribution. In the La_2CrCoO_6 (LCCO) and La_2CrNiO_6 (LCNO) compounds, Cr has the maximum contribution to the total spin magnetic moment, whereas in the La_2ScNiO_6 (LSNO) and La_2VNiO_6 (LVNO) compounds, Ni has the maximum contribution. However, in the case of the La_2VScO_6 (LVSO) compound, V has the maximum contribution to the total spin magnetic moment. Furthermore, in all these compounds La_2CrNiO_6 (LCNO) has the maximum total spin magnetic moment of 4.0 μ_B, whereas La_2ScNiO_6 (LSNO) has the minimum total magnetic moment of 0.9 μ_B.

Table 2 The magnetic moments of half-metallic ferromagnetic (HM-FM) double perovskites, along with interstitial region (m^{Intst}), individual atom (m^{S1}, m^{S2}, m^{S3}, m^{S4}, m^{S5}) and total cell (m^{Cell}) magnetic moments by GGA calculation

Serial no.	Materials	m^{Intst}	m^{S1}	m^{S2}	m^{S3}	m^{S4}	m^{S5}	m^{Cell}
1	La_2CrCoO_6	0.27150	0.01201	2.32582	0.18412	0.01326	0.01290	2.88359
2	La_2CrNiO_6	0.28269	0.01420	1.99849	1.38930	0.04885	0.05090	4.00017
3	La_2ScNiO_6	0.01170	−0.00220	0.04520	0.77638	0.02802	0.02834	0.99828
4	La_2VNiO_6	0.15326	0.01338	0.89250	1.48145	0.06907	0.06982	2.97139
5	La_2VScO_6	0.42797	0.07356	1.42382	0.03688	−0.00487	−0.00447	2.00820

Table 3 The magnetic moments of half-metallic ferromagnetic (HM-FM) double perovskites, along with interstitial region (m^{Intst}), individual atom (m^{S1}, m^{S2}, m^{S3}, m^{S4}, m^{S5}) and total cell (m^{Cell}) magnetic moments by GGA (+U) calculation

Serial no.	Compound	m^{Intst}	m^{S1}	m^{S2}	m^{S3}	m^{S4}	m^{S5}	m^{Cell}
1	La$_2$CrCoO$_6$	0.32371	0.02128	2.38831	0.15488	0.01886	0.01511	3.00761
2	La$_2$CrNiO$_6$	0.26399	0.01282	1.97414	1.40242	0.05606	0.05715	4.00693
3	La$_2$ScNiO$_6$	−0.01631	0.00239	0.01728	1.31964	−0.05725	−0.05270	1.00007
4	La$_2$VNiO$_6$	0.15399	0.01325	0.89531	1.48322	0.06848	0.06922	2.97283
5	La$_2$VScO$_6$	0.42984	0.07343	1.42780	0.03685	−0.00532	−0.00506	2.01050

3.3. Optical properties

We have investigated the optical properties of the half-metallic ferromagnetic ordered double perovskite compounds La$_2$CrCoO$_6$, La$_2$CrNiO$_6$, La$_2$ScNiO$_6$, La$_2$VNiO$_6$ and La$_2$VScO$_6$, including the optical conductivity $\sigma(\omega)$, reflectivity $R(\omega)$, refractive index $n(\omega)$, absorption co-efficient $\alpha(\omega)$ and real $\varepsilon_1(\omega)$ and imaginary $\varepsilon_2(\omega)$ parts of the dielectric constant for various energies (in eV), via the GGA and GGA (+U) techniques. The calculated optical conductivity ($\sigma(\omega)$) is illustrated in Fig. 5(a and b). The optical conductivity ($\sigma(\omega)$) is the ratio of the current density to the electric field and depends on the frequency or energy of the incident photons, and is represented by the equation:

$$\sigma(\omega) = J(\omega)/E(\omega) \tag{1}$$

The calculated values of the optical conductivity ($\sigma(\omega)$) are listed in Table 4, and show that the optical conductivity ($\sigma(\omega)$) varies from 11.205 to 14.927. La$_2$CrCoO$_6$ (LCCO) has the maximum value of 14.927 at 20.993 eV, whereas La$_2$ScNiO$_6$ (LSNO) has the minimum value of 11.205 at 21.565 eV. The values of the optical conductivity calculated by using the GGA scheme for the La$_2$CrCoO$_6$, La$_2$CrNiO$_6$, La$_2$ScNiO$_6$, La$_2$VNiO$_6$ and La$_2$VScO$_6$ compounds are 14.927, 14.181, 11.205, 14.377 and 11.680 at 20.993 eV, 20.911 eV, 21.565 eV, 20.830 eV and 20.367 eV. The values of the optical conductivity using the GGA
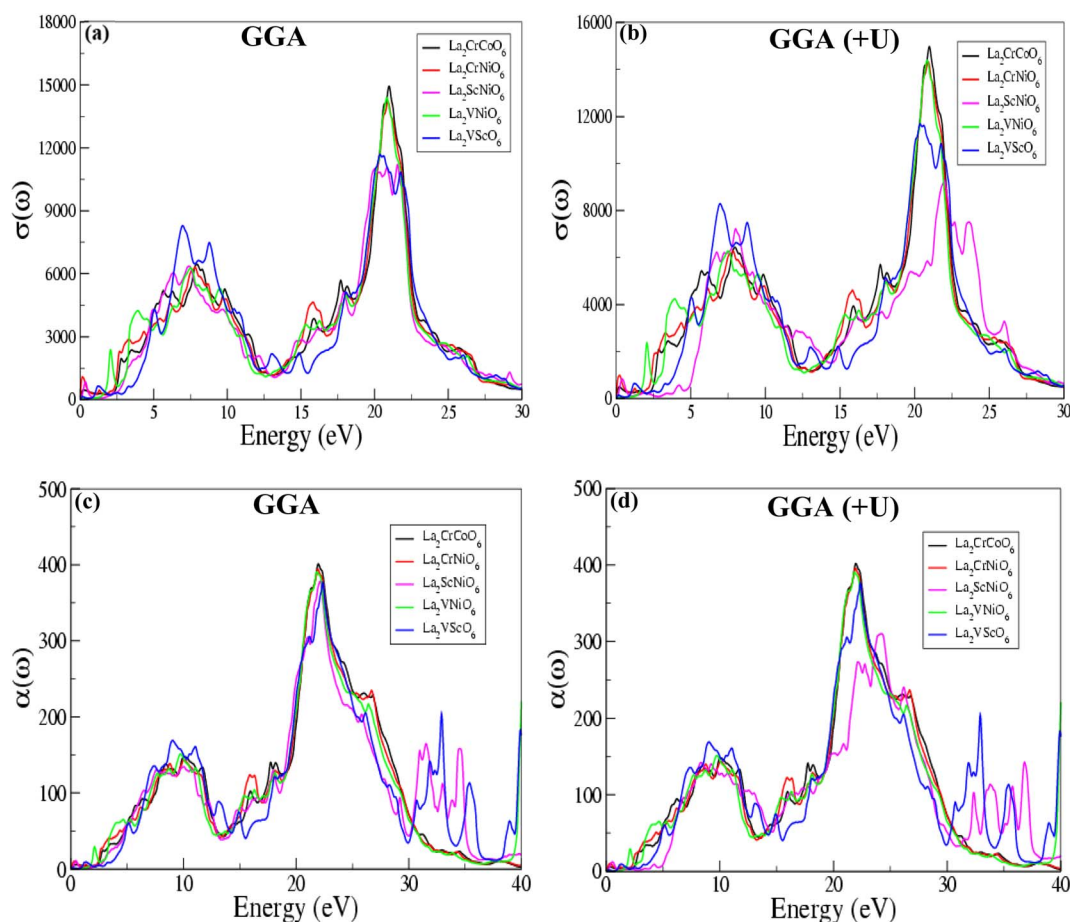
Fig. 5 (a, b) Optical conductivity ($\sigma(\omega)$) and (c, d) absorption co-efficient ($\alpha(\omega)$) of the La$_2$CrCoO$_6$, La$_2$CrNiO$_6$, La$_2$ScNiO$_6$, La$_2$VNiO$_6$ and La$_2$VScO$_6$ compounds calculated by the GGA and GGA (+U) processes.

Table 4 The optical conductivities $\sigma(\omega)$ and absorption co-efficients $\alpha(\omega)$ of the half-metallic ferromagnetic (HM-FM) double perovskite compounds, calculated by the GGA and GGA (+U) schemes

Serial no.	Compound	GGA		GGA (+U)		GGA		GGA (+U)	
		$\sigma(\omega)$	E (eV)	$\sigma(\omega)$	E (eV)	$\alpha(\omega)$	E (eV)	$\alpha(\omega)$	E (eV)
1	La_2CrCoO_6	14.927	20.993	14.958	20.990	401.082	21.973	401.871	21.973
2	La_2CrNiO_6	14.181	20.911	14.317	20.912	394.128	21.918	395.603	21.918
3	La_2ScNiO_6	11.205	21.565	9.286	22.000	378.128	22.136	376.096	22.204
4	La_2VNiO_6	14.377	20.830	14.377	20.830	390.602	21.837	390.602	21.837
5	La_2VScO_6	11.680	20.367	11.680	20.367	376.535	22.354	376.535	22.535

(+U) scheme for the La_2CrCoO_6, La_2CrNiO_6, La_2ScNiO_6, La_2VNiO_6 and La_2VScO_6 compounds are 14.958, 14.317, 9.286, 14.377 and 11.680 at 20.990 eV, 20.912 eV, 22.000 eV, 20.830 eV and 20.367 eV. The results obtained for the optical conductivity are nearly the same for both the GGA and GGA (+U) techniques. Furthermore, the value of the optical conductivity ($\sigma(\omega)$) for La_2VNiO_6 (LVNO) and La_2VScO_6 (LVSO) is exactly same for both schemes. The absorption coefficients $\alpha(\omega)$ calculated for the La_2CrCoO_6, La_2CrNiO_6, La_2ScNiO_6, La_2VNiO_6 and La_2VScO_6 compounds shown in Fig. 5(c and d) quantify the incident light absorbed by the material (instead of being reflected or

refracted), giving information about the transformation of electromagnetic energy into the internal energy of the absorber.

The values of the absorption coefficient $\alpha(\omega)$ calculated *via* GGA and GGA (+U) listed in Table 4 indicate that of all five of these compounds, La_2CrCoO_6 (LCCO) has the maximum value of 401.082 at 21.973 eV, showing that this compound has more potential to absorb incident photons and can be used for absorption in optical devices.

The absorption power for incident photons in the La_2VScO_6 compound is the minimum (376.535 at 22.354 eV), indicating that this compound may be less useful for optical and
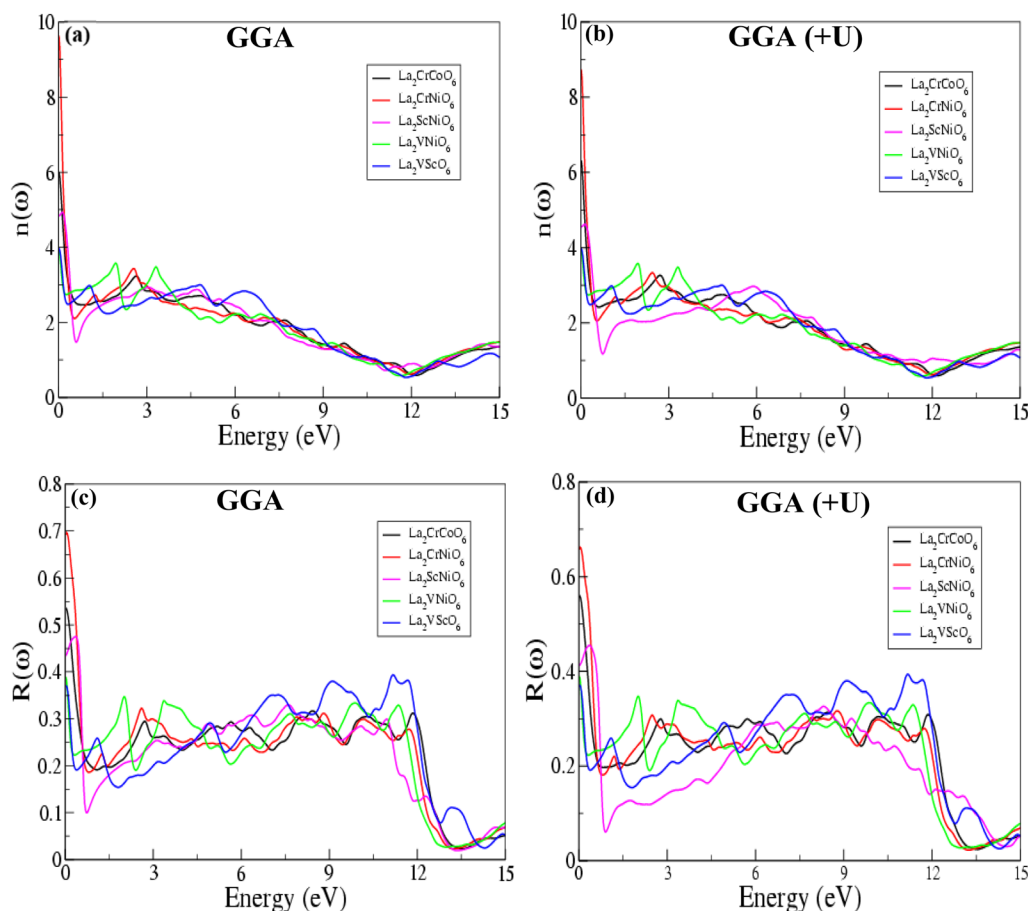
Fig. 6 (a, b) Refractive index ($n(\omega)$) and (c, d) reflectivity $R(\omega)$ of the La_2CrCoO_6, La_2CrNiO_6, La_2ScNiO_6, La_2VNiO_6 and La_2VScO_6 compounds calculated by the GGA and GGA (+U) processes.
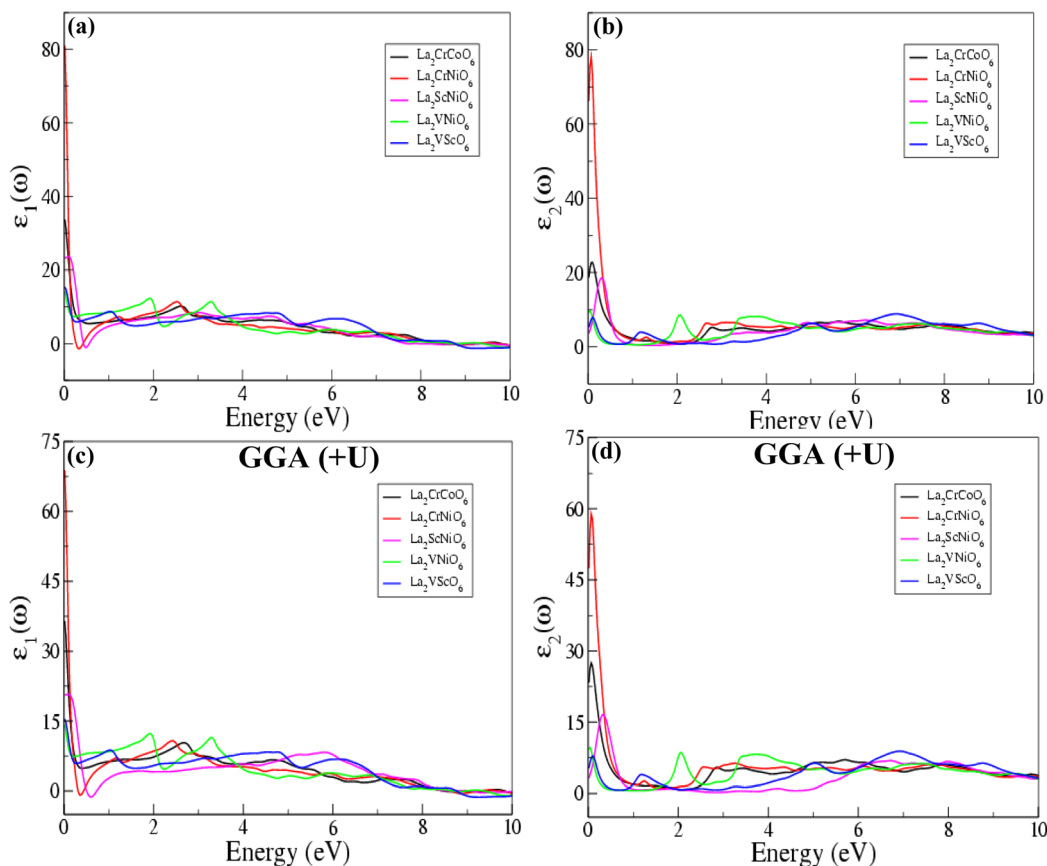
Fig. 7 Real $\varepsilon_1(\omega)$ and imaginary $\varepsilon_2(\omega)$ parts of the dielectric constants of the La$_2$CrCoO$_6$, La$_2$CrNiO$_6$, La$_2$ScNiO$_6$, La$_2$VNiO$_6$ and La$_2$VScO$_6$ compounds calculated by the GGA and GGA (+U) processes.

optoelectronic applications than the other four compounds. The value of the energy observed for the maximum absorption coefficient ($\alpha(\omega)$) is in the range of 21 eV to 22.5 eV. Interestingly, the absorption coefficient ($\alpha(\omega)$) calculated for La$_2$VNiO$_6$ is $\alpha = 390.602$, exactly the same for both schemes, and both schemes exhibit the same value of the energy ($E = 21.837$ eV). The values of the optical absorption coefficients $\alpha(\omega)$ are specific for each compound, validating the potential application in optics where a specific ultraviolet radiation (UV) wavelength of absorption is required, such as in sunglasses, colored filters, dyes *etc.*

Fig. 6 represents the refractive indices ($n(\omega)$) of all five compounds. The refractive index $n(\omega)$ is a critical feature of semiconductors, revealing the amount of light bent or refracted. The value of $n(\omega)$ increases with increasing energy (eV). The GGA and GGA (+U) calculations report higher values of the refractive index $n(\omega)$ for La$_2$CrCoO$_6$, La$_2$CrNiO$_6$, La$_2$ScNiO$_6$, La$_2$VNiO$_6$ and La$_2$VScO$_6$ compounds of 6.005 (at 0.013 eV), 9.602 (at 0.038 eV), 4.928 (at 0.122 eV), 3.943 (at 0.013 eV) and 3.979 (at 0.013 eV), and 6.322 (at 0.013 eV), 8.732 (at 0.013 eV), 4.614 (at 0.149 eV), 3.820 (at 0.019 eV) and 3.979 (at 0.013 eV), indicating their potential use in optoelectronic applications, primarily in electronic displays, such as LCDs, OLEDs, and quantum dot (QDLED) televisions. The refractive index ($n(\omega)$) calculated for La$_2$CrNiO$_6$ has the maximum value of 9.602 at 0.038 eV, whereas

a minimum value of 3.943 at 0.013 eV is reported for the La$_2$VNiO$_6$ compound, as compared to the other compounds. There is no large difference between the refractive indices ($n(\omega)$) calculated by GGA and GGA (+U). The refractive indices ($n(\omega)$) measured for the La$_2$VNiO$_6$ and La$_2$VScO$_6$ compounds are nearly the same at 0.013 eV in the GGA scheme. The refractive indices ($n(\omega)$) of La$_2$CrCoO$_6$ and La$_2$ScNiO$_6$ are equal to 6.0 and 4.9 at 0.013 eV and 0.122 eV, respectively. The $n(\omega)$ values observed for all these compounds are non-linear. Initially there is a sharp increase and then a decrease with increasing energy (eV), *etc.*, which is in good agreement with previously reported theoretical and experimental results related to 2D double perovskites.[40–44]

The optical reflectivity $R(\omega)$ values in relation to the incident energy calculated *via* GGA and GGA (+U) shown Fig. 6(c and d) confirm the reflective nature of these compounds. The optical reflectivity $R(\omega)$ is the ratio of the energy of a wave reflected from a surface to the energy possessed by the wave striking the surface. The GGA and GGA (+U) values of the reflectivity $R(\omega)$ for the La$_2$CrCoO$_6$, La$_2$CrNiO$_6$, La$_2$ScNiO$_6$, La$_2$VNiO$_6$ and La$_2$VScO$_6$ compounds of 0.534, 0.696, 0.475, 0.389 and 0.369, and 0.558, 0.662, 0.454, 0.389 and 0.369 indicate that the surfaces of these materials are smooth and have an ordered crystalline structure. Among all five of these compounds, La$_2$CrNiO$_6$ has the maximum value of 0.696 at 0.04 eV, whereas La$_2$VScO$_6$ has the

lowest value of 0.369 at 0.013 eV in both the GGA and GGA (+U) schemes.

The calculated real $\varepsilon_1(\omega)$ and imaginary $\varepsilon_2(\omega)$ parts of the dielectric constant as a function of energy (eV) calculated *via* both the GGA and GGA (+U) schemes are shown in Fig. 7. The dielectric constant, known as the relativity permittivity or specific inductive capacity, is a dimensionless number expressing a material's ability to support an electrostatic field while dissipating a minimum amount of energy in the form of heat. The calculated values of the static dielectric constants for the La$_2$CrCoO$_6$, La$_2$CrNiO$_6$, La$_2$ScNiO$_6$, La$_2$VNiO$_6$ and La$_2$VScO$_6$ compounds confirm that all these compounds display a dielectric response, and according to GGA approximations the values of the real parts of the dielectric constant $\varepsilon_1(\omega)$ are in the range of 14.172 to 80.617, and the values of the imaginary parts are in the range of 7.867 to 78.097. Furthermore, according to the GGA (+U) scheme, the values of the real parts of the dielectric constant $\varepsilon_1(\omega)$ are in the range of 14.172 to 68.613, and the values of the imaginary parts $\varepsilon_2(\omega)$ are in the range of 7.867 to 58.682.

It is worth noting that the value of the $\varepsilon_2(\omega)$ is zero until absorption starts after the photon energy reaches the band gap energy, which determines the threshold for a direct optical transition between the VBM and the CBM. The dielectric constant values describe the effect of the electric field on a material and the higher the dielectric constant, the more the material tends to reduce any field set up in it. In both the GGA and GGA (+U) processes, the calculated values of the real $\varepsilon_1(\omega)$ and imaginary $\varepsilon_2(\omega)$ parts of the dielectric constant for La$_2$-CrNiO$_6$ (LCNO) are the highest, which indicates that this material is more dielectric than the others. La$_2$VNiO$_6$ (LVNO) is the least dielectric material, indicated by the obtained values of the dielectric constant. The materials with high dielectric constants are useful in the manufacture of high-value capacitors.

4. Conclusions

In this study, we investigated the influence of 3d transition metal incorporation at the B (Cr and V) and B$'$ (Co, Ni and Sc) sites of the 2D La$_2$BB$'$O$_6$ double perovskites on the electronic, magnetic, and optoelectronic properties. Full structural optimization was carried out by using the full-potential linearized augmented plane wave technique as implemented in WIEN2K software. The results are in good agreement with previously reported work. The electronic band structures in the spin-up and spin-down states reveal that all five of these compounds are half-metallic. In the case of the spin-up channel, La$_2$CrCoO$_6$, La$_2$CrNiO$_6$, La$_2$ScNiO$_6$, La$_2$VNiO$_6$ and La$_2$VScO$_6$ display metallic features, while they display non-metallic features in the spin-down channel. The calculated density of states gives a detailed explanation of the band structure, and the electronic distributions of these compounds drawn in terms of the total density of states verify the half-metallic nature. The pd-hybridizations, double exchange correlations (strong-correlation correction (GGA (+U))), ground-state energies and calculated total magnetic moments (2.9 μ_B, 2.0 μ_B, 0.9 μ_B, 4.0 μ_B

and 2.8 μ_B) of these compounds confirm the ferromagnetic behavior. Therefore, the overall nature of these materials is half-metallic ferromagnetic. We have calculated the optical conductivities $\sigma(\omega)$ and absorption co-efficients $\alpha(\omega)$, and the maximum values are 14.927 and 401.08 at 21.97 eV for the La$_2$CrCoO$_6$ compound. The refractive index ($n(\omega)$) and optical reflectivity ($R(\omega)$) calculations reveal that La$_2$CrNiO$_6$ has the highest values of 9.602 at 0.038 eV and 0.696 at 0.04 eV, whereas La$_2$VNiO$_6$ has the lowest values of 3.943 at 0.013 eV and 0.389 at 0.013 eV, compared to all the other compounds. The real and imaginary parts of the dielectric constant show that La$_2$CrNiO$_6$ has the maximum value, which means that this compound is more dielectric than the others. The fully spin-polarized strong magnetic element induces the weak magnetic element, and slightly increases the positive (or negative) magnetic moment, therefore it is regarded as the main cause of the half-metallic properties. In summary, based on our calculations, we revealed that 2D La$_2$BB$'$O$_6$ double perovskites with 3d transition metals incorporated at the B (Cr and V) and B$'$ (Co, Ni and Sc) sites have potential applications in spintronic, multifunctional, and optoelectronic devices.

Data availability

The raw/processed data required to reproduce these findings cannot be shared at this time as the data also forms part of an ongoing study. The data may be provided on request.

Conflicts of interest

I hereby confirm that the work reported in this manuscript is novel and has no conflict of interest.

Acknowledgements

References

1 J. Zhu, H. Li, L. Zhong, P. Xiao, X. Xu, X. Yang, Z. Zhao and J. Li, Perovskite oxides: preparation, characterizations, and applications in heterogeneous catalysis, *ACS Catal.*, 2014, **4**(9), 2917–2940.

2 *Properties and Applications of Perovskite-Type Oxides*, ed. L. G. Tejuca and J. L. Fierro, CRC Press, 2000.

3 E. Grabowska, Selected perovskite oxides: characterization, preparation and photocatalytic properties—a review, *Appl. Catal., B*, 2016, **186**, 97–126.

4 M. Acosta, N. Novak, V. Rojas, S. Patel, R. Vaish, J. Koruza, G. A. Rossetti Jr and J. Rödel, BaTiO$_3$-based piezoelectrics: fundamentals, current status, and perspectives, *Appl. Phys. Rev.*, 2017, **4**, 041305.

5 P. Wang, Q. Guo, F. Li, F. Xia, H. Hao, H. Sun, H. Liu and S. Zhang, Modified Pb(Mg$_{1/3}$Nb$_{2/3}$)O$_3$-PbZrO$_3$–PbTiO$_3$

ceramics with high piezoelectricity and temperature stability, *J. Am. Ceram. Soc.*, 2021, **104**(10), 5127–5137.

6 Q. Guo, F. Li, F. Xia, X. Gao, P. Wang, H. Hao, H. Sun, H. Liu and S. Zhang, High-performance Sm-doped $Pb(Mg_{1/3}Nb_{2/3})O_3$-$PbZrO_3$-$PbTiO_3$-based piezoceramics, *ACS Appl. Mater. Interfaces*, 2019, **11**(46), 43359–43367.

7 C. J. Howard, B. J. Kennedy and P. M. Woodward, Ordered double perovskites – a group-theoretical analysis, *Acta Crystallogr., Sect. B: Struct. Sci.*, 2003, **59**(4), 463–471.

8 A. E. Maughan, A. M. Ganose, D. O. Scanlon and J. R. Neilson, Perspectives and design principles of vacancy-ordered double perovskite halide semiconductors, *Chem. Mater.*, 2019, **31**(4), 1184–1195.

9 S. Nazir, Insulator-to-half metal transition and enhancement of structural distortions in [… formula…] double perovskite oxide *via* hole-doping, *Sci. Rep.*, 2021, **11**, 1240.

10 H. Kato, T. Okuda, Y. Okimoto, Y. Tomioka, K. Oikawa, T. Kamiyama and Y. Tokura, Metal-insulator transition of ferromagnetic ordered double perovskites:$(Sr_{1-y}Ca_y)_2FeReO_6$, *Phys. Rev. B: Condens. Matter Mater. Phys.*, 2002, **65**(14), 144404.

11 W. Prellier, V. Smolyaninova, A. Biswas, C. Galley, R. L. Greene, K. Ramesha and J. Gopalakrishnan, Properties of the ferrimagnetic double perovskites A_2FeReO_6 (A = Ba and Ca), *J. Phys.: Condens. Matter*, 2000, **12**(6), 965.

12 I. V. Solovyev, Electronic structure and stability of the ferrimagnetic ordering in double perovskites, *Phys. Rev. B: Condens. Matter Mater. Phys.*, 2002, **65**(14), 144446.

13 M. Hashisaka, D. Kan, A. Masuno, M. Takano, Y. Shimakawa, T. Terashima and K. Mibu, Epitaxial growth of ferromagnetic La_2NiMnO_6 with ordered double-perovskite structure, *Appl. Phys. Lett.*, 2006, **89**(3), 032504.

14 E. Carvajal, O. Navarro, R. Allub, M. Avignon and B. Alascio, Ferromagnetic transition in ordered double perovskites and related alloys, *Eur. Phys. J. B*, 2005, **48**(2), 179–187.

15 D. D. Russell, A. J. Neer, B. C. Melot and S. Derakhshan, Long-range antiferromagnetic ordering in b-site ordered double perovskite Ca_2ScOsO_6, *Inorg. Chem.*, 2016, **55**(5), 2240–2245.

16 L. Ortega-San Martin, J. P. Chapman, L. Lezama, J. Sánchez Marcos, J. Rodríguez-Fernández, M. I. Arriortua and T. Rojo, Magnetic properties of the ordered double perovskite Sr_2MnTeO_6, *Eur. J. Inorg. Chem.*, 2006, **7**, 1362–1370.

17 M. R. Li, M. Retuerto, Z. Deng, P. W. Stephens, M. Croft, Q. Huang, H. Wu, X. Deng, G. Kotliar, J. Sánchez-Benítez and J. Hadermann, Giant magnetoresistance in the half-metallic double-perovskite ferrimagnet Mn_2FeReO_6, *Angew. Chem., Int. Ed.*, 2015, **54**(41), 12069–12073.

18 F. Estrada, E. J. Guzmán, O. Navarro and M. Avignon, Curie temperature behavior in half-metallic ferromagnetic double perovskites within the electronic correlation picture, *Phys. Rev. B*, 2018, **97**(19), 195155.

19 O. Erten, O. N. Meetei, A. Mukherjee, M. Randeria, N. Trivedi and P. Woodward, Theory of half-metallic ferrimagnetism in double perovskites, *Phys. Rev. Lett.*, 2011, **107**(25), 257201.

20 Q. Tang and X. Zhu, Half-metallic double perovskite oxides: recent developments and future perspectives, *J. Mater. Chem. C*, 2022, 15301–15338.

21 N. Rahmani, M. E. Ghazi, M. Izadifard, D. Wang, A. Shabani and B. Sanyal, Density functional study of structural, electronic and magnetic properties of new half-metallic ferromagnetic double perovskite Sr_2MnVO_6, *J. Phys.: Condens. Matter*, 2019, **31**(47), 475501.

22 O. N. Meetei, O. Erten, A. Mukherjee, M. Randeria, N. Trivedi and P. Woodward, Theory of half-metallic double perovskites. I. Double exchange mechanism, *Phys. Rev. B: Condens. Matter Mater. Phys.*, 2013, **87**(16), 165104.

23 Q. Tang and X. Zhu, Half-metallic double perovskite oxides: recent developments and future perspectives, *J. Mater. Chem. C*, 2022, 15301–15338.

24 G. M. Mustafa, M. Hassan, N. M. Aloufi, S. Saba, S. Al-Qaisi, Q. Mahmood, H. Albalawi, S. Bouzgarrou, H. H. Somaily and A. Mera, Half metallic ferroamgnetism, and transport properties of vacancy ordered double perovskites $Rb_2(Os/Ir)X_6$ (X = Cl, Br) for spintronic applications, *Ceram. Int.*, 2022, 23460–23467.

25 T. Alshahrani, Q. Mahmood and M. Rashid, The role of 5d electrons spin in quantum ferromagnetism and transport properties of double perovskites Cs_2ZCl/Br_6 (Z = Ta, W) for spintronic applications, *Eur. Phys. J. Plus*, 2021, **136**(3), 1–2.

26 J. B. Philipp, P. Majewski, L. Alff, A. Erb, R. Gross, T. Graf, M. S. Brandt, J. Simon, T. Walther, W. Mader, D. Topwal and D. D. Sarma, Structural and doping effects in the half-metallic double perovskite A_2CrWO_6 (A =Sr, Ba, and Ca), *Phys. Rev. B: Condens. Matter Mater. Phys.*, 2003 Oct, **68**, 144431.

27 Y. P. Liu, S. H. Chen, H. R. Fuh and Y. K. Wang, First-principle calculations of half-metallic double perovskite $La_2BB'O_6$ (B, B' = 3d transition metal), *Commun. Comput. Phys.*, 2013, **14**(1), 174–185.

28 U. R. Mehtab, W. Qun and Y. Yunfei, Electronic, Magnetic and Optical Properties of Double Perovskite Compounds: A First Principle Approach, *Crystals*, 2022, **12**(11), 1597.

29 J. H. Park, S. K. Kwon and B. I. Min, Half-metallic antiferromagnetic double perovskites: $LaAVRuO_6$ (A = Ca, Sr, and Ba), *Phys. Rev. B: Condens. Matter Mater. Phys.*, 2002, **65**(17), 174401.

30 S. H. Chen, Z. R. Xiao, P. H. Lee, Y. P. Liu and Y. K. Wang, Stability of half-metallic antiferromagnet La_2VMnO_6, first-principles calculation study, *Phys. B*, 2011, **406**(14), 2783–2787.

31 D. D. Sarma, E. V. Sampathkumaran, S. Ray, R. Nagarajan, S. Majumdar, A. Kumar, G. Nalini and T. G. Row, Magnetoresistance in ordered and disordered double perovskite oxide, Sr_2FeMoO_6, *Solid State Commun.*, 2000, **114**(9), 465–468.

32 J. P. Perdew, K. Burke and M. Ernzerhof, Generalized gradient approximation made simple, *Phys. Rev. Lett.*, 1996, **77**(18), 3865.

33 K. Burke, J. P. Perdew and M. Ernzerhof, Why the generalized gradient approximation works and how to go beyond it, *Int. J. Quantum Chem.*, 1997, **61**(2), 287–293.

34 Z. Wu and R. E. Cohen, More accurate generalized gradient approximation for solids, *Phys. Rev. B: Condens. Matter Mater. Phys.*, 2006, **73**(23), 235116.

35 S. Bo and Z. Ping, First-principles local density approximation (LDA) + U and generalized gradient approximation (GGA) + U studies of plutonium oxides, *Chin. Phys. B*, 2008, **17**(4), 1364.

36 Y. Guermit, M. Drief, T. Lantri, A. Tagrerout, H. Rached, N. E. Benkhettou and D. Rached, Theoretical investigation of magnetic, electronic, thermoelectric and thermodynamic properties of Fe_2TaZ (Z = B, In) compounds by GGA and GGA + U approaches, *Comput. Condens. Matter*, 2020, **22**, e00438.

37 S. A. Mir and D. C. Gupta, Understanding the origin of half-metallicity and thermophysical properties of ductile La_2CuMnO_6 double perovskite, *Int. J. Energy Res.*, 2019, **43**(9), 4783–4796.

38 S. Satpathy, Z. S. Popović and F. R. Vukajlović, Density-functional studies of the electronic structure of the perovskite oxides: $La_{1-x}Ca_x MnO_3$, *J. Appl. Phys.*, 1996, **79**(8), 4555–4557.

39 M. U. Rehman, Q. Wang and Y. Yu, Electronic, Magnetic and Optical Properties of Double Perovskite Compounds: A First Principle Approach, *Crystals*, 2022, **12**(11), 1597.

40 S. Berri, N. Bouarissa, M. Ibrir and O. Meglali, Optical spectra and thermal properties of double perovskite Ba_2LuTaO_6 material, *Optik*, 2021, **229**, 166272.

41 S. A. Dar, R. Sharma, V. Srivastava and U. K. Sakalle, Investigation on the electronic structure, optical, elastic, mechanical, thermodynamic and thermoelectric properties of wide band gap semiconductor double perovskite Ba_2InTaO_6, *RSC Adv.*, 2019, **9**(17), 9522–9532.

42 M. Hussain, M. Rashid, A. Ali, M. F. Bhopal and A. S. Bhatti, Systematic study of optoelectronic and transport properties of cesium lead halide (Cs_2PbX_6; X = Cl, Br, I) double perovskites for solar cell applications, *Ceram. Int.*, 2020, **46**(13), 21378–21387.

43 O. T. Ali, M. R. Mohamed, M. H. Ali, M. E. Elsayed and B. Mikhael, Optical, electrical and magnetic properties of lanthanum strontium manganite $La_{1-x}Sr_xMnO_3$ synthesized through the citrate combustion method, *Phys. Chem. Chem. Phys.*, 2017, **19**, 6878–6886.

44 I. Koriba, B. Lagoun, A. Cheriet, G. Abdenacer, B. Soraya, A. Anfel, A. Linda and A. Akram, Phase stability, mechanical and optoelectronic properties of lanthanum chromite-based perovskite oxide, *Appl. Phys. A*, 2022, **128**, 82.